Research article

NMR IN BIOMEDICINE

Received: 18 February 2013, Revised: 27 June 2013, Accepted: 28 June 2013, Published online in Wiley Online Library: 15 August 2013

(wileyonlinelibrary.com) DOI: 10.1002/nbm.3005

Hyperpolarized singlet lifetimes of pyruvate in human blood and in the mouse

Irene Marco-Rius[a], Michael C. D. Tayler[b], Mikko I. Kettunen[a], Timothy J. Larkin[a], Kerstin N. Timm[a], Eva M. Serrao[a], Tiago B. Rodrigues[a], Giuseppe Pileio[b], Jan Henrik Ardenkjaer-Larsen[c], Malcolm H. Levitt[b] and Kevin M. Brindle[a]*

Hyperpolarized NMR is a promising technique for non-invasive imaging of tissue metabolism *in vivo*. However, the pathways that can be studied are limited by the fast T_1 decay of the nuclear spin order. In metabolites containing pairs of coupled nuclear spins-1/2, the spin order may be maintained by exploiting the non-magnetic singlet (spin-0) state of the pair. This may allow preservation of the hyperpolarization *in vivo* during transport to tissues of interest, such as tumors, or to detect slower metabolic reactions. We show here that in human blood and in a mouse *in vivo* at millitesla fields the ^{13}C singlet lifetime of [1,2-$^{13}C_2$]pyruvate was significantly longer than the ^{13}C T_1, although it was shorter than the T_1 at field strengths of several tesla. We also examine the singlet-derived NMR spectrum observed for hyperpolarized [1,2-$^{13}C_2$]lactate, originating from the metabolism of [1,2-$^{13}C_2$]pyruvate. © 2013 The Authors. *NMR in Biomedicine* published by John Wiley & Sons, Ltd.

Keywords: blood; dynamic nuclear polarization; pyruvate; lactate; long-lived states; longitudinal relaxation time; relaxation; hyperpolarization

INTRODUCTION

There is growing interest in tumor cell metabolism and an appreciation of its importance in cancer cell biology (1–3). Non-invasive imaging techniques of cancer cell metabolism, which include positron emission tomography (PET) and MRS, have provided novel approaches for detecting disease and response to treatment, as well as increasing our knowledge of cancer biology (2–9). High temporal and spatial resolution measurements of enzyme-catalyzed reactions *in vivo* are possible using dissolution dynamic nuclear polarization (dissolution DNP) enhanced MRS. This technique allows the full nuclear spin magnetization to be exploited, which provides signals up to 10^4 times stronger than from thermal equilibrium magnetization (10). Several ^{13}C-labeled molecules have been successfully hyperpolarized and their metabolism imaged *in vivo* (2,7).

The most widely used substrate to date is [1-^{13}C]pyruvate, due to the high polarization that can be obtained and the long T_1 of the carboxyl carbon relative to its rates of cellular uptake and subsequent metabolism ($T_1 \sim 30$ s *in vivo* in magnetic fields above 1 T) (2). Pyruvate is the end product of the glycolytic pathway and may be reversibly converted to lactate and alanine in the reactions catalyzed by lactate dehydrogenase and alanine aminotransferase, respectively. Measurements of the interconversion of pyruvate and lactate, which is fast relative to the T_1 of the hyperpolarized ^{13}C label, have been used for tumor grading and detection of treatment response (5,8,9,11).

Pyruvate is well tolerated when injected intravenously, and a clinical trial of hyperpolarized [1-^{13}C]pyruvate in prostate cancer has been completed recently (12). However, the relatively short lifetime of the hyperpolarized signal remains a significant limitation, and compounds in which the hyperpolarized ^{13}C label has a longer lifetime would be of great value in the clinical setting. For instance, this would provide more time for handling the substrate prior to injection into a patient, and reduce relaxation-induced signal losses during circulation in the blood stream.

The upper limit of the spin polarization lifetime of an isolated spin-1/2 nucleus (such as the carboxyl carbon in [1-$^{13}C_1$]pyruvate) is the longitudinal relaxation time T_1. In spin-1/2 pairs, however, longer relaxation times are possible for the singlet configuration $|S_0\rangle = (|\alpha_1\beta_2\rangle - |\beta_1\alpha_2\rangle)/\sqrt{2}$. The population of $|S_0\rangle$ decays with a time constant denoted T_S, which may exceed

* *Correspondence to: Kevin M. Brindle, Department of Biochemistry, University of Cambridge, UK, and Cancer Research UK Cambridge Research Institute, Cambridge, UK.*
E-mail: kmb1001@cam.ac.uk

a *I. Marco-Rius, M. I. Kettunen, T. J. Larkin, K. N. Timm, E. M. Serrao, T. B. Rodrigues, K. M. Brindle*
Department of Biochemistry, University of Cambridge, UK, and Cancer Research UK Cambridge Research Institute, Cambridge, UK

b *M. C. D. Tayler, G. Pileio, M. H. Levitt*
Department of Chemistry, University of Southampton, UK

c *J. H. Ardenkjaer-Larsen*
GE Healthcare, Copenhagen, Denmark

Abbreviations used: *PET, positron emission tomography; DNP, dynamic nuclear polarization; BSA, bovine serum albumin; PBS, phosphate-buffered saline; T_S, singlet relaxation time constant; J, J-coupling constant (in Hz); ω^0, Larmor frequency of the nucleus of interest (in rad/s); γ, gyromagnetic ratio of the nucleus of interest (in rad/Ts); δ, chemical shift of the nucleus of interest (in ppm); B, magnetic field strength (in tesla); p, longitudinal polarization.*

T_1 by an order of magnitude. In general $T_S > T_1$ arises only in the regime of near magnetic equivalence between the spin pair, namely in the strong-coupling limit $|\Delta\omega^0| \ll |\pi J|$, where (i) the singlet and triplet spin states of the pair are stationary with respect to coherent evolution, and (ii) symmetric relaxation mechanisms are symmetry forbidden. We have reported previously on the long-lived ^{13}C singlet state in [1,2-$^{13}C_2$]pyruvate in solution at a laboratory magnetic field, $B^{0(LF)}$, that satisfied the condition $|\Delta\omega^0| = |\gamma_C B^{0(LF)}\,\Delta\delta_C| \ll |\pi J_{CC}|$ (13). Studies of the relaxation of singlet order in $^{15}N_2O$ in blood have also been reported (14). We examine here what, if any, benefits there would be in creating singlet order in [1,2-$^{13}C_2$]pyruvate for studies *in vivo* by investigating the singlet state of [1,2-^{13}C]pyruvate in whole human blood and in the mouse. The results obtained are, to our knowledge, the first showing singlet-order derived signal *in vivo*.

THEORY

There are several well established methods available for preparing hyperpolarized singlet order starting from longitudinal spin order, at both low and high magnetic fields (15–18). In this work, however, we employ an alternative approach that exploits singlet order available in the hyperpolarized state immediately after dissolution DNP. This approach is illustrated in Figure 1, where frozen hyperpolarized material is dissolved and transported adiabatically into a region of low magnetic field. Singlet order proportional to the square of the longitudinal polarization is generated from the excess population of the Zeeman states $|\alpha_1\alpha_2\rangle$ and $|\beta_1\beta_2\rangle$ relative to $|\alpha_1\beta_2\rangle$ and $|\beta_1\alpha_2\rangle$. For a weakly coupled spin pair with positive gyromagnetic ratio γ, positive chemical shift difference $(\delta_2 - \delta_1)$ and positive intra-pair scalar coupling J, the

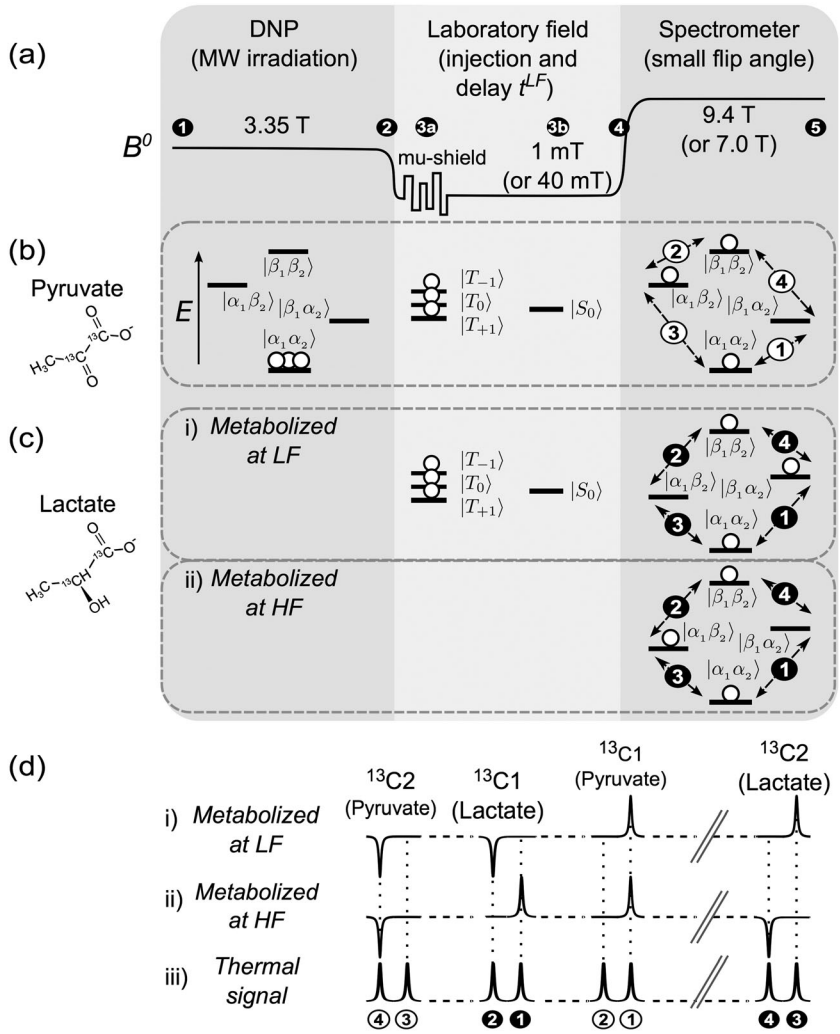

Figure 1. (a) Experimental sequence for hyperpolarized singlet NMR of [1,2-$^{13}C_2$]pyruvate. (1, 2) Dissolution DNP of the sample is followed by manipulations in low magnetic field. (3a) Option of shaking the sample inside a magnetically shielded chamber, which rapidly dephases non-singlet spin order. (3b) Injection into the biological system at low field. (4, 5) After waiting in the low field, the sample is then shuttled into a high-field spectrometer for NMR signal readout. (b) Illustration of the excess in $|\alpha_1\alpha_2\rangle$ population of the hyperpolarized substrate, which generates singlet depletion order upon dissolution and transfer to low magnetic field. Pure singlet order remains after the triplet states equilibrate via rapid T_1 relaxation in the low field, or are dephased using a mu-metal chamber. Following a small-tip-angle excitation pulse, the resulting spectrum contains a pair of peaks in anti-phase. (c) Fate of the singlet order in [1,2-$^{13}C_2$]pyruvate after metabolism to [1,2-$^{13}C_2$]lactate. Different outcomes are predicted depending on whether metabolism takes place at high or low magnetic field, since the chemical shift difference has opposite sign in the two molecules. (d) The resulting spectral patterns. For reference, the peak pattern of a sample in thermal equilibrium is shown in (iii).

high-field and low-field eigenstates correlate as follows:

$$\begin{aligned} &|\alpha_1\alpha_2\rangle \leftrightarrow |T_{+1}\rangle \\ &|\alpha_1\beta_2\rangle \leftrightarrow |T_0\rangle = 1/2(|\alpha_1\beta_2\rangle + |\beta_1\alpha_2\rangle) \\ &|\beta_1\beta_2\rangle \leftrightarrow |T_{-1}\rangle \\ &|\beta_1\alpha_2\rangle \leftrightarrow |S_0\rangle = 1/2(|\alpha_1\beta_2\rangle - |\beta_1\alpha_2\rangle) \end{aligned} \quad [1]$$

For a reversed sign in any of the parameters J, $(\delta_2 - \delta_1)$ and γ the states $|\alpha_1\beta_2\rangle$ and $|\beta_1\alpha_2\rangle$ correlate the opposite way around:

$$\begin{aligned} &|\alpha_1\alpha_2\rangle \leftrightarrow |T_{+1}\rangle \\ &|\beta_1\alpha_2\rangle \leftrightarrow |T_0\rangle = 1/2(|\alpha_1\beta_2\rangle + |\beta_1\alpha_2\rangle) \\ &|\beta_1\beta_2\rangle \leftrightarrow |T_{-1}\rangle \\ &|\alpha_1\beta_2\rangle \leftrightarrow |S_0\rangle = 1/2(|\alpha_1\beta_2\rangle - |\beta_1\alpha_2\rangle) \end{aligned} \quad [2]$$

High-field polarization followed by adiabatic transport to low field leads to a depletion in the population of $|S_0\rangle$, the amplitude of which is proportional to p^2, for longitudinal polarization p, as demonstrated in (13). We stress that, while the singlet order obtained by this approach is much lower than that accessible by converting the longitudinal polarization using a pulse sequence at low field, such as the one described by Pileio *et al*. (16) (about 2.4/p lower), the simpler preparation route used here was sufficient for the demonstrations presented in this work. However, conversion of all available spin order into singlet order, with the attendant increase in measured signal, would be an advantage in a clinical setting.

The population difference between the triplet states tends to thermal equilibrium with the longitudinal relaxation time constant T_1^{LF} of the low field. Meanwhile, the depleted singlet population equalizes with the time constant T_S, which in favorable circumstances may be longer. Figure 1(b) (middle panel) shows the system configuration assuming $T_S > T_1^{LF}$ after the triplet populations have reached equilibrium. A simple yet effective procedure that allows one to selectively observe NMR signals resulting from singlet spin order is to shake the sample in a magnetically shielded chamber, which rapidly dephases all other spin order (Fig. 1(a)). The mu-metal cylinder distorts magnetic flux lines to its surface, resulting in an extremely inhomogeneous and weak fluctuating magnetic field in the neighboring space (13). Shaking the sample modulates this field, the result of which is to rapidly dephase spin order with non-zero spherical rank. Conventional magnetization, which is spin order of spherical rank 1 and higher, is averaged, leaving only singlet order (spherical rank 0).

The characteristic spectrum of a spin system with singlet order in which the triplet populations are equilibrated at low field, or are filtered out by using the magnetically shielded chamber, contains two outer transitions when acquired with a small-flip-angle r.f. pulse, as shown in Figure 2(b)(ii). The two peaks have equal areas but are opposite in sign. This contrasts with all four transitions occurring in phase (same sign) following a small-flip-angle pulse applied to pure longitudinal order (Fig. 2(b)(i)). If the sample is inserted into the spectrometer before the triplet populations have equilibrated and a small-flip-angle spectrum is acquired, two asymmetric doublets will be obtained (Fig. 2(b)(iii)). The two contributions to the spectrum can be separated from one another: the total area under the spectrum is proportional to the longitudinal magnetization present, while the difference between the areas under each doublet is characteristic of the singlet order.

Following injection of hyperpolarized [1,2-$^{13}C_2$]pyruvate into a mouse, the pair of ^{13}C nuclei of the product of any metabolic reaction will also be expected to be in singlet order configuration, provided that the chemical bond between the two ^{13}C nuclei is preserved and that the field is sufficiently low to satisfy the

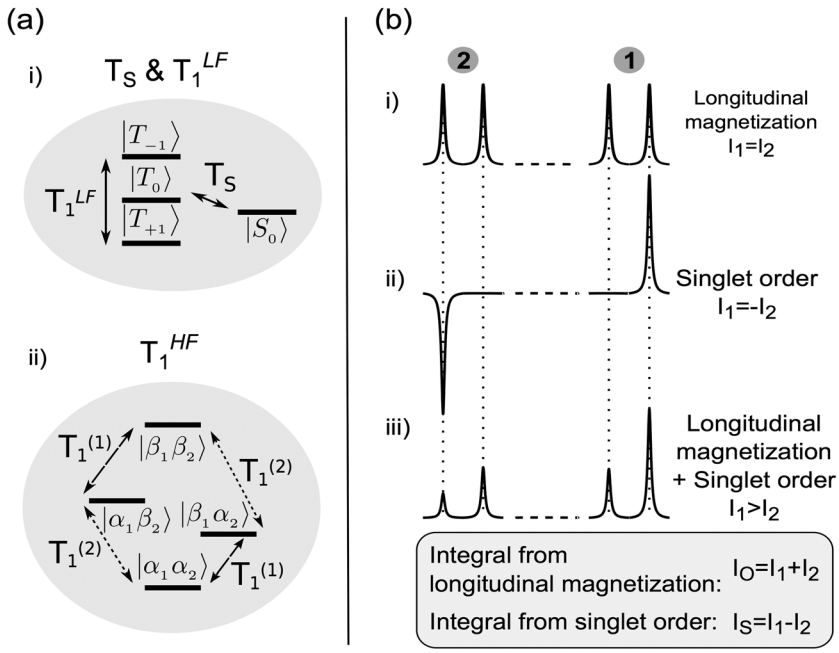

Figure 2. (a) Relaxation of a spin-1/2 pair at high and low magnetic fields. (i) At low field (triplet–singlet configuration, or near-magnetic-equivalence regime), the triplet populations relax with a single exponential time constant T_1^{LF}, while the singlet population relaxes with a potentially slower time constant T_S. (ii) At high magnetic field (Zeeman configuration, or weak-coupling regime), each nucleus of the pair relaxes with its own distinct T_1. (b) Illustration of the spectral signatures obtained after placing the system in high field, arising from (i) longitudinal spin order, (ii) singlet order or (iii) both. By adding or subtracting the peak integrals I_1 and I_2, one may distinguish the contribution of each of (i) and (ii) to the spectrum (see text).

near-equivalence condition ($|\Delta\omega^0| \ll |\pi J_{CC}|$). Hyperpolarized [1,2-$^{13}C_2$]pyruvate can be converted into [1,2-$^{13}C_2$]lactate. There are different spectral outcomes for [1,2-$^{13}C_2$]lactate depending on whether the enzymatic reaction occurs at low or high magnetic field, since the chemical shift difference ($\delta_2 - \delta_1$) for [1,2-$^{13}C_2$]lactate has opposite sign to that for [1,2-$^{13}C_2$]pyruvate:

(1) Metabolic conversion at low field (Fig. 1(c)(i)) generates singlet-depleted $^{13}C_2$-lactate. According to Equation [2] the state after transfer into high magnetic field corresponds to a depleted population of $|\alpha_1\beta_2\rangle$, since for lactate ($\delta_2 - \delta_1$) < 0). The small-flip-angle spectrum contains one positive peak from the $|\alpha_1\alpha_2\rangle$ to $|\alpha_1\beta_2\rangle$ transition and one negative peak from the $|\beta_1\beta_2\rangle$ to $|\alpha_1\beta_2\rangle$ transition. This should be contrasted with the singlet-derived NMR signal from [1,2-$^{13}C_2$]pyruvate, which gives a positive peak for the $|\alpha_1\alpha_2\rangle$ to $|\beta_1\alpha_2\rangle$ transition and a negative peak for the $|\beta_1\beta_2\rangle$ to $|\beta_1\alpha_2\rangle$ transition, under the same circumstances.

(2) During transport from low to high magnetic field, the singlet order of [1,2-$^{13}C_2$]pyruvate is transferred into a population depletion of $|\beta_1\alpha_2\rangle$ (Fig. 1(b)). Subsequent metabolic conversion then results in [1,2-$^{13}C_2$]lactate depleted in $|\beta_1\alpha_2\rangle$, in contrast to the low-field metabolic postcursor (Fig. 1(c)(ii)). The small-flip-angle spectrum contains one positive peak for the $|\alpha_1\alpha_2\rangle$ to $|\beta_1\alpha_2\rangle$ transition and a negative peak for the $|\beta_1\beta_2\rangle$ to $|\beta_1\alpha_2\rangle$ transition (Fig. 1(d)(ii)). Similar reasoning explains the expected peak pattern from [1,2-$^{13}C_2$]pyruvate hydrate, which has also a chemical shift difference ($\delta_2 - \delta_1$) with opposite sign to that for [1,2-$^{13}C_2$]pyruvate. However, if the bond is broken, for example as occurs during the decarboxylation of pyruvate to form carbon dioxide in the reaction catalyzed by pyruvate dehydrogenase, the product metabolite will display zero NMR signal, since the correlation of its angular momentum is lost entirely.

METHODS

Sample preparation and hyperpolarization

[1,2-$^{13}C_2$]pyruvic acid (99% purum) and [1-^{13}C]pyruvic acid (95% purum) were purchased from Sigma (Dorset, Gillingham, UK). Samples were prepared using 43.5 mg of pyruvic acid, 0.7 mg of trityl radical OX063 (GE Healthcare, Little Chalfont, UK) and 1.2 mg of a 1:10 gadolinium chelate (gadoteric acid, Dotarem®; Guerbet, Roissy, France) solution, and were placed in a GE Healthcare DNP prototype hyperpolarizer working at 3.35 T and ~1.2 K. The frozen sample was irradiated for 1 h with 100 mW microwaves at 93.972 GHz. The material was then dissolved in a superheated buffer solution (~180 °C, ~1 MPa) containing 100 mg/L ethylenediaminetetraacetic acid (EDTA), 30 mM NaCl, 94 mM NaOH and 40 mM 4-(2-hydroxyethyl)-1-piperazineethanesulfonic acid (HEPES) dissolved in D_2O.

For *in vivo* experiments, the hyperpolarization step was carried out using a Hypersense instrument (Oxford BioTools, Oxford, UK), otherwise following the same procedure as described above.

MRS of hyperpolarized pyruvate in whole blood

Immediately after dissolution DNP, 2 mL of the hyperpolarized pyruvate solution were injected into 10 mL of whole human blood contained in a 50 mL Falcon tube, giving a final pyruvate concentration of 13.5 mM. An optional step of oxygenating the blood was performed prior to this mixing by passing O_2 gas through the void space of the Falcon tube while gently swirling to encourage the gas to dissolve. Oxygen was flushed until no further change in the color of the blood was observed (approximately 2.5 min).

For measurement of T_1 and T_S at low field, 3 mL aliquots of the blood–pyruvate solution were transferred into three 10 mm o.d. NMR tubes. These were placed in a water bath at 37 °C in the laboratory field (~1 mT). At intervals of approximately 20 s the tubes were inserted sequentially into a 9.4 T vertical wide-bore magnet (100 MHz ^{13}C, Oxford Instruments, Oxford, UK) interfaced with a Varian ^{Unity}Inova spectrometer console (Varian Inc., Palo Alto, CA). For each tube, six ^{13}C 6°-flip-angle spectra were acquired at intervals of 1 s, with the probe maintained at 37 °C. T_S and T_1^{LF} were determined by fitting to the sum and difference of the spectrum integrals, as outlined above.

To measure T_1^{HF}, a 0.5 mL aliquot of the dissolved pyruvate sample was injected by a transfer line into a tube containing 2.5 mL blood inside the 9.4 T magnet (resulting in a 3 mL sample volume with the same final pyruvate concentration, 13.5 mM, as the low-field experiments). Polarization decay was determined by measuring sixty 6°-flip-angle spectra at intervals of 1 s and fitting an exponential to the spectrum integrals.

The ^{13}C nuclear polarization was determined by comparing the hyperpolarized NMR signals with a spectrum of one of the tubes after complete decay of the hyperpolarization. This thermal equilibrium spectrum was acquired using a 6°-flip-angle pulse, and 128 transients with a repetition time of 60 s. The polarization was estimated to be approximately ~20 % at the time of injection, approximately 10 s after dissolution.

MRS of hyperpolarized pyruvate in solutions of bovine serum albumin

Hyperpolarized [1,2-$^{13}C_2$]pyruvate was added to phosphate-buffered saline (PBS) solutions containing 0%, 1%, 2%, 3% or 5% (w/v) bovine serum albumin (BSA) to give a final pyruvate concentration of 13.5 mM. The pH of each BSA solution was 7.0 ± 0.1 after addition of the hyperpolarized pyruvate. Aliquots (2.5 mL) of each BSA solution were added to five 10 mm o.d. NMR tubes and maintained at 37 °C. The tubes were then inserted sequentially into the 9.4 T magnet at 30 s intervals to measure T_1^{LF} and T_S^{LF}. For each tube, fourteen 6°-flip-angle ^{13}C spectra were acquired at intervals of 1 s, with the tubes maintained at 37 °C, to measure T_1^{HF}.

Measurements of the stray field of the 9.4 T and the 7.0 T magnets

The magnetic field at the locations where the hyperpolarized samples were stored was measured using a transverse Hall probe in combination with a hand-held gaussmeter (HIRST GM04, Magnetic Instruments, Falmouth, Cormwall, UK).

Cell culture

EL-4 murine lymphoma cells were grown to a density of circa 5×10^7 cells/mL in RPMI 1640 medium supplemented with 10% (v/v) fetal calf serum and 2 mM glutamine.

Tumor implantation

C57/Blk6 female mice (6–8 weeks old) were injected subcutaneously with 100 μL of a suspension of 5×10^6 EL4 cells in the left flank and tumors were allowed to grow for 11 days, by which

time they were ~2 cm^3 in volume. Tumor development and mouse well-being were assessed by regular measurements of tumor size and by visual inspection, respectively. All experiments were performed under the Animals (Scientific Procedures) Act of 1986 and were approved by local ethical review committees.

Nuclear magnetic resonance spectroscopy *in vivo*

Animals were anesthetized prior to NMR experiments by administration of a mixture containing O_2 in medical air (25%/75% v/v at 2 L/min) plus 3% isoflurane (Isoflo, Abbotts Laboratories, Maidenhead, Berkshire, UK) and subsequently 1–2% isoflurane in O_2/medical air. They were then placed in a temperature-regulated, dual-tuned $^{13}C/^{1}H$ volume coil for ^{13}C transmit and for ^{1}H transmit and receive, and a 20 mm diameter surface coil for ^{13}C receive only (Rapid Biomedical, Rimpar, Germany). The core body temperature of the animal was maintained at ~37 °C. The surface coil was placed immediately over the tumor so that it detected signal that was principally from the tumor. Respiratory rate and body temperature were monitored using a Biotrig physiological monitor (Small Animal Instruments, Stony Brook, NY, USA). A cannula was inserted into a tail vein and its patency maintained through the use of heparin diluted in sterile saline (100 U/mL).

The hyperpolarized [1,2-$^{13}C_2$]pyruvate solution (0.2 mL, approximately 80 mM) was injected intravenously over a period of 3–5 s in a low magnetic field of approximately 40 mT. After injection, the mouse and probe assembly were rapidly shuttled into a 7 T horizontal bore magnet (Varian, Palo Alto, CA, USA) for signal acquisition. Spectra were acquired using a non-slice-selective excitation pulse (600 μs sinc-pulse with a nominal bandwidth of 10 kHz) with a flip angle of 10°. A maximum of two injections were given to each mouse.

As a diagnostic of singlet order, in one experiment an animal was injected with singlet-filtered hyperpolarized [1,2-$^{13}C_2$]pyruvate. After dissolution, the pyruvate solution was shaken inside a mu-metal cylinder for approximately 5 s, in order to destroy the longitudinal magnetization. The solution was then injected (~ 25 s after dissolution) and spectra acquired as described above.

Data analysis

Data were processed using *Mathematica* (Wolfram, Champaign, IL, USA). NMR signals were zero filled from 6 k to 16 k (blood) or from 1 k to 8 k data points (*in vivo*), Fourier transformed and the baselines corrected.

The relaxation time constants were estimated by fitting mono-exponential decay curves to the peak integrals. For [1-^{13}C]pyruvate, the value of T_1^{HF} refers to the longitudinal decay constant at 9.4 T, while T_1^{LF} corresponds to the decay constant at 1 mT. For measurements at low field, multiple samples were maintained at low field for varying periods of time before being inserted into the 9.4 T magnet for measurement. For [1,2-$^{13}C_2$]pyruvate, the C1 and the C2 doublets in the first spectrum from each tube were integrated separately and the areas processed according to the sum and difference method (Fig. 2(b)). The sum gives the longitudinal magnetization while the difference gives the singlet order. These values for longitudinal magnetization and singlet order from successive tubes were fitted to obtain T_1^{LF} and T_S, respectively. Additional estimates of T_1^{LF} and T_S were obtained from the integrals from the second and subsequent spectra from each tube, until the magnetization had decayed, and these values were then averaged. However, the values quoted are the averages from the specified number of independent experiments. For experiments at high field the integrals of the C1 and C2 doublets were fitted to an exponential decay function to obtain T_1^{HF} for each site. Quoted errors are the standard errors on the mean.

RESULTS

T_S and T_1 of pyruvate in whole blood at 1 mT and 9.4 T

Figure 3(a) shows an NMR spectrum acquired immediately after addition of hyperpolarized [1,2-$^{13}C_2$]pyruvate to an NMR tube containing oxygenated human blood that was already in the 9.4 T spectrometer magnet, the sample being injected via a transfer line. This spectrum comprises two asymmetric doublets, indicating the presence of both hyperpolarized longitudinal magnetization and singlet order in a ratio of 16:1.

The spectrum shown in Figure 3(b) resulted from addition of hyperpolarized pyruvate to blood with the sample being kept in a low field (1 mT) for 16 s prior to signal acquisition. In this case, the multiplet pattern consists of only the anti-phase outer peaks, and indicates that only singlet-derived spin order was present at the time of signal acquisition. This was evidence that the singlet order decayed slowly relative to the longitudinal magnetization, i.e the singlet was "long lived", at low field. The data obtained in all the experiments with oxygenated and non-oxygenated blood suggested that, at ~1 mT, T_1^{LF} was less than 5 s (after ~20 s only singlet order was detected in the spectra). However, the time interval at which the tubes could be inserted into the acquisition magnet was 15–20 s, so accurate quantification was not possible. The longer lifetime of the singlet order, T_S, was estimated to be ~19 s, and no differences in the fitted relaxation times between oxygenated and non-oxygenated blood were observed.

The fitted time constants T_1 and T_S for [1-$^{13}C_2$]pyruvate and [1,2-$^{13}C_2$]pyruvate in whole human blood are summarized in

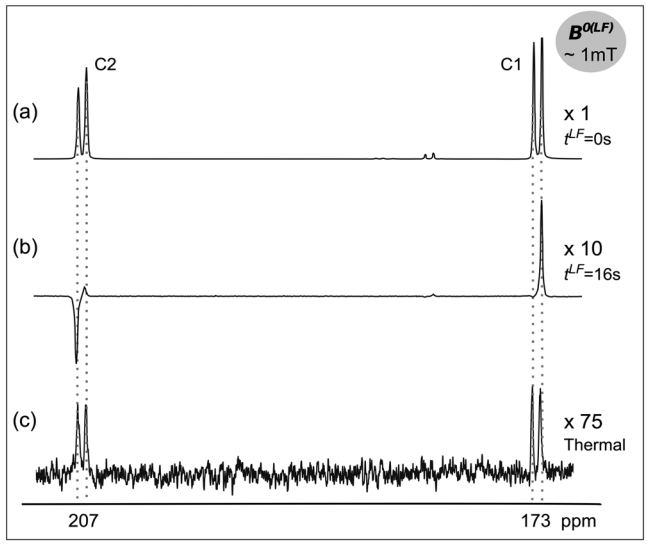

Figure 3. ^{13}C NMR spectra of 13.5 mM hyperpolarized [1,2-$^{13}C_2$]pyruvate in oxygenated, whole human blood (a) immediately after injection (1 scan) and (b) 16 s after injection and maintenance at 1 mT (1 scan); (c) the same sample at thermal equilibrium (128 scans, $T_R = 1$ s). Spectra were acquired at 9.4 T and 37 °C using a 6° flip angle pulse.

Table 1. ^{13}C relaxation time constants of hyperpolarized [1,2-$^{13}C_2$]pyruvate and [1-^{13}C]pyruvate in whole human blood at 37 °C

	T_1^{LF} (s) at 1 mT	T_S (s) at 1 mT	T_1^{HF} (s) at 9.4 T
[1,2-$^{13}C_2$]pyruvate (non-oxygenated, $n = 3$)	<5	17 ± 2	38.5 ± 0.4 (C1), 30.0 ± 0.2 (C2)
[1,2-$^{13}C_2$]pyruvate (oxygenated, $n = 4$)	<5	19 ± 2	38.3 ± 0.5 (C1), 30.6 ± 0.3 (C2)
[1-^{13}C]pyruvate (non-oxygenated, $n = 2$)	8 ± 1	N.A.	45.0 ± 0.5
[1-^{13}C]pyruvate (oxygenated, $n = 2$)	9 ± 2	N.A.	40 ± 2

Table 1. At 9.4 T the ^{13}C T_1^{HF} values for [1,2-$^{13}C_2$]pyruvate were shorter than that measured for [1-^{13}C]pyruvate. For both isotopologues the ^{13}C T_1^{LF} values at 1 mT were almost an order of magnitude shorter than the respective values of T_1^{HF}. The T_S for [1,2-$^{13}C_2$]pyruvate at 1 mT was approximately four times longer than T_1^{LF} of the same system. However, T_S at low field was half T_1^{HF} measured at 9.4 T. Oxygenating the blood had no apparent effect on the measured relaxation times.

Experiments in BSA solutions at 1 mT and 9.4 T

The relaxation behavior of [1,2-$^{13}C_2$]pyruvate in whole blood may be explained by interaction of pyruvate with serum proteins. To investigate this, relaxation time constants for [1,2-$^{13}C_2$]pyruvate in aqueous PBS solutions containing 0, 1, 2, 3 and 5% (w/v) BSA were measured (Table 2) (human blood contains between 3.5 and 5% serum albumin). The decay of the signal in BSA solutions was slower than in blood, and T_1^{HF} could be measured in the same experiment as T_1^{LF} by acquiring 14 spectra at 9.4 T from the same tube with a flip angle of 6° and a repetition time of 1 s. The data show significant shortening of T_1^{LF} at 1% BSA (~50% of T_1^{LF} without BSA), with further decreases at 2, 3 and 5% BSA (at 5% BSA T_1^{LF} was ~30% of that at 0% BSA), whereas at high field T_1^{HF} was largely independent of BSA concentration between 0 and 5%. Albeit less dramatic, T_S also decreased as the protein concentration increased. At 5% BSA, T_S was ~2 times T_1^{LF} and almost as long as T_1^{HF} of the C2 carbon, although still only ~60% of T_1^{HF} of the C1 carbon. The changes in the inverse relaxation time constants, or relaxation rates, with BSA concentration are shown in Figure 4. An approximately linear increase of the longitudinal relaxation rates ($\tau_1 = 1/T_1$) with BSA concentration was observed. Importantly, $1/T_1$ increased faster than the singlet relaxation rate $1/T_S$, demonstrating that the singlet order is less sensitive to relaxation induced by BSA than the longitudinal magnetization.

Observation of the singlet state *in vivo*

Figure 5 shows a set of spectra obtained *in vivo* from a murine tumor model following tail vein injection of hyperpolarized [1,2-$^{13}C_2$]pyruvate, where the mice were maintained at ~40 mT for different periods of time. The spectra were similar to those observed in blood (Fig. 3), although an additional feature was the appearance of peaks corresponding to [1,2-$^{13}C_2$]lactate due to metabolism of [1,2-$^{13}C_2$]pyruvate. In the spectrum acquired from the mouse immediately after the injection of [1,2-$^{13}C_2$]pyruvate (~18 s after dissolution; $t^{LF} \sim 0$ s in the figure), singlet order was evident in the asymmetry of the doublets from the pyruvate C1 and C2 carbons. The pyruvate was injected while the animal was outside the magnet, and it was then shuttled rapidly into the magnet. The asymmetry in the pyruvate C1 and C2 carbons was also observed in the C1 carbon of lactate at 183 ppm and the C1 carbon of pyruvate hydrate at 181 ppm (Fig. 5(a)). The experiment was repeated in the same mouse 1 h later, except that the animal was maintained at low field for ~7 s after injection (Fig. 5(b), $t^{LF} \sim 7$ s). The resulting pyruvate spectrum from the tumor showed pure singlet order (Fig. 5(b)). Likewise, the characteristic anti-phase peak pattern was also evident when the mouse was maintained at low field for ~3 s after injection (data not shown). This indicated that the longitudinal magnetization relaxed much faster at low field than the singlet order, and was consistent with the data obtained in whole blood and in BSA solutions at low field. A spectrum acquired after injection of hyperpolarized [1,2-$^{13}C_2$]pyruvate, in which longitudinal magnetization had been destroyed by shaking the sample inside a mu-metal chamber, again only showed signal from the negative singlet order in pyruvate (Fig. 5(c)). In this case the pyruvate was injected at ~30 s after dissolution.

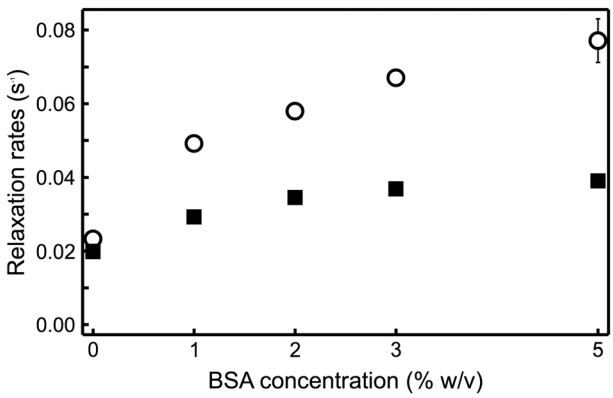

Figure 4. Dependence of relaxation rates $R_1^{LF} = 1/T_1^{LF}$ (○) and $R_S = 1/T_S$ (■) on the concentration of BSA in aqueous solution (data from Table 2).

Table 2. Relaxation time constants ^{13}C in hyperpolarized [1,2-$^{13}C_2$]pyruvate at different concentrations of BSA in PBS at pH = 7 and 37 °C ($n = 2$)

	0% BSA	1% BSA	2% BSA	3% BSA	5% BSA
T_1^{LF} (s) at 1 mT	43.3 ± 0.6	20.4 ± 0.2	17.3 ± 0.3	14.9 ± 0.4	13 ± 1
T_S (s) at 1 mT	50 ± 3	34 ± 1	28.8 ± 0.5	27 ± 1	25.5 ± 1
T_1^{HF} (s) at 9.4 T (C1, C2)	46.0 ± 0.5, 32 ± 1	44 ± 4, 33.5 ± 0.3	42 ± 2, 36.9 ± 0.4	40 ± 1, 34 ± 2	40 ± 1, 28 ± 3

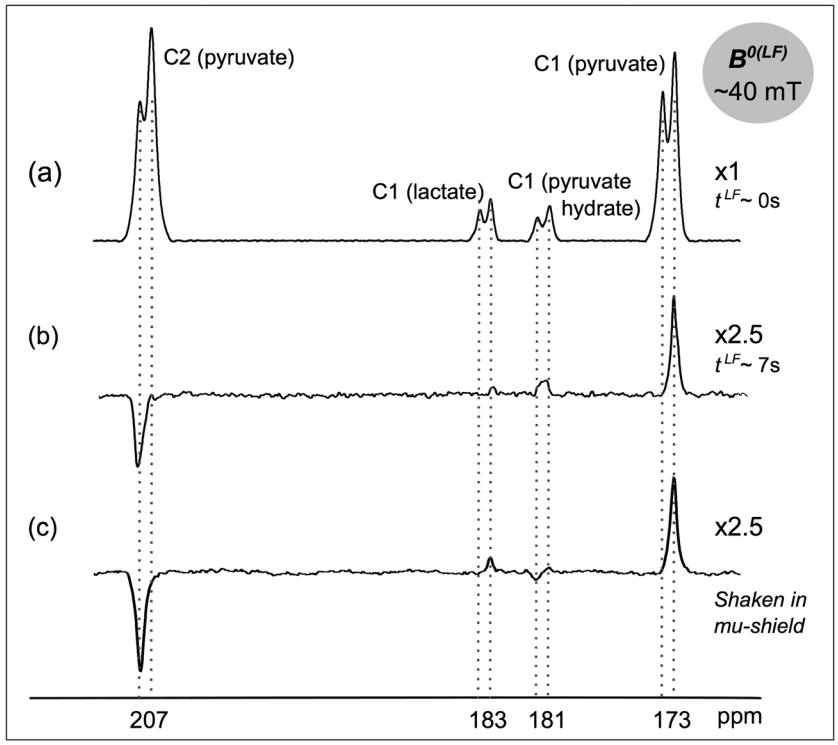

Figure 5. ^{13}C NMR spectra from a mouse tumor *in vivo* at 7.0 T following i.v. injection of hyperpolarized [1,2-$^{13}C_2$]pyruvate, acquired (a) immediately following injection (~18 s after dissolution), (b) after maintaining the animal for ~7 s at ~40 mT after injection and (c) following injection of hyperpolarized pyruvate prepared with negative singlet order (~30 s after dissolution; the longitudinal magnetization of the sample was destroyed by shaking the hyperpolarized substrate in a mu-metal chamber immediately after dissolution). In all three experiments the spectra were acquired with a single scan.

DISCUSSION

By boosting the polarization of a pair of coupled spin-1/2 nuclei using DNP, the hyperpolarized signal displays negative singlet order without further manipulation of the spin system. The sensitivity of the experiment could be improved by the use of pulse sequences at low field that increase the singlet state population (16,19).

The peak asymmetry arising from the spectrum of a coupled spin-pair has been used previously as a method of estimating longitudinal nuclear polarization (20–22). However, estimation of the polarization using the peak asymmetry is problematic, considering the variation of T_1 and T_S with magnetic field strength observed here.

The change in T_1 between high and low fields may result from binding of pyruvate to blood proteins, resulting in a reduction of the molecule's mobility and, therefore, a change in correlation time. To investigate this, the effect of different BSA concentrations on T_1^{LF} and T_S of [1,2-$^{13}C_2$]pyruvate was determined. BSA has almost identical effects to oxyhemoglobin on the proton T_1 of water (23), and for the range of BSA concentrations studied here the changes in T_1 cannot be attributed to a viscosity effect (24). Similar to the results presented by Pullinger *et al*. (25) on the T_1 relaxation time of hyperpolarized [1-^{13}C]pyruvate in BSA, we found that at low field (~1 mT) T_1^{LF}, and also T_S, decreased markedly in a 1% BSA solution; increasing the BSA concentration further had only modest effects (Table 2). A 1% BSA solution corresponds to a protein concentration of ~0.2 mM. The smaller decrease in T_1^{LF} and T_S at higher BSA concentrations may reflect saturation of the binding sites for pyruvate. At high field (9.4 T) the T_1^{HF} for [1,2-$^{13}C_2$]pyruvate was largely independent of BSA concentration (Table 2). Moreno *et al*. reported that, at 14.1 T, the T_1^{HF} of [1-^{13}C]pyruvate decreased with increasing BSA concentration, finding T_1 values much shorter than those we measured at 9.4 T (26). The discrepancy with what we observed here for [1,2-$^{13}C_2$]pyruvate might be explained by a greater contribution of chemical shift anisotropy to T_1^{HF} at 14.1 T.

T_1^{LF} for [1,2-$^{13}C_2$]pyruvate in 5% BSA was ~2.5 times longer than T_1^{LF} in whole blood (which contains human serum albumin), whereas T_S was only ~1.3 times longer. The faster T_1^{LF} relaxation in blood may reflect the presence of paramagnetic species (27). However, it appears from our experiments that such an effect cannot be attributed to the presence of deoxyhemoglobin, since the use of partially deoxygenated blood had no apparent effect on the measured values of T_1^{LF}, T_S or T_1^{HF}. The oxygenation level of blood and hence the ratio of oxy- to deoxyhemoglobin, the latter being moderately paramagnetic, has been shown to cause larger changes in T_2 as compared with T_1 (23,28). Consistent with our observations, it has been reported previously that water proton T_1 is not affected by hemoglobin oxygenation but that it does change with magnetic field strength (29).

The higher T_S/T_1^{LF} ratio measured in blood, as compared with that measured in BSA solutions, may reflect the contribution of other paramagnetic species in blood to T_1^{LF} relaxation, since these have been shown to have a weaker effect on the relaxation of singlet order (30).

Consistent with the longer values measured for T_S as compared with T_1^{LF} in whole blood and solutions of BSA at ~1 mT, our results also show that T_S of [1,2-$^{13}C_2$]pyruvate was longer than T_1^{LF} at ~40 mT in a live mouse. If hyperpolarized singlet order [1,2-$^{13}C_2$]pyruvate is injected into a subject and this subject is maintained at low magnetic field, the ^{13}C nuclei of the product

of any metabolic reaction will also be expected to be in singlet order configuration, provided that the chemical bond between the two carbons is preserved and that the field is sufficiently low to satisfy the near-equivalence condition (Fig. 1(c)). Our observations show that singlet order was not preserved in the product [1,2-$^{13}C_2$]lactate produced at 40 mT from the injected [1,2-$^{13}C_2$]pyruvate. Comparing with the spectral outcomes predicted in Figure 1(d)(ii), we concluded that the lactate signal arises from metabolism at high magnetic field, not low field.

The absence of NMR signals from singlet [1,2-$^{13}C_2$]lactate may be explained by the relatively large chemical shift difference between the carbon sites ($|\delta_1 - \delta_2| \sim 114$ ppm), which at 40 mT corresponds to a frequency difference of 50 Hz. This contrasts with pyruvate, where $|\delta_1 - \delta_2|$ is only ~15 Hz at 40 mT. The 50 Hz frequency difference is not negligible when compared with the 60 Hz coupling constant J_{C1C2} in lactate, and means that the singlet and triplet states of lactate are no longer eigenstates of the coherent Hamiltonian. The resulting evolution is an efficient mechanism for singlet leakage, such that one should expect the lifetime T_S of singlet-polarized lactate to be similar to T_1, and shorter than it might potentially be if the singlet were an eigenstate. In addition, the presence of a C2 proton in lactate introduces a strong heteronuclear coupling, as well as an asymmetric relaxation mechanism due to the large difference in the H2–C1 and H2–C2 dipole–dipole couplings, further accelerating the decay of singlet order.

Consequently, if [1,2-$^{13}C_2$]pyruvate is injected at ~40 mT and the mouse is maintained at this field while conversion of pyruvate to lactate occurs, then singlet polarization in pyruvate will leak through into non-singlet polarization in lactate. Therefore, at the moment of detection an apparent reduction in the amount of lactate will be observed in the spectra (Fig. 5(b)). Even if one could reduce the field at which the mouse is maintained during injection to 10 mT, the singlet–triplet states would still not be pure eigenstates of the Hamiltonian and singlet polarization decay would still be accelerated in the lactate product.

Similar reasoning can explain the observed spectral patterns for [1,2-$^{13}C_2$]pyruvate hydrate ($|\delta_1 - \delta_2| \sim 85$ ppm). The spectrum shown in Figure 5(b) is characteristic of [1,2-$^{13}C_2$]pyruvate hydrate formed at high field, which is consistent with the relatively rapid injection of [1,2-$^{13}C_2$]pyruvate into the mouse at 40 mT field and spectrum acquisition at 7 T. The spectrum in Figure 5 (c), on the other hand, shows signals from pyruvate hydrate formed in both low (negative peak of the doublet) and high fields (positive peak of the doublet). In this experiment the solution was shaken in the mu-metal chamber prior to injection into the animal and transport into the 7 T magnet. During this singlet preparation time pyruvate and pyruvate hydrate may undergo chemical exchange at a low field, where the eigenstates of both molecules are in the singlet and triplet states. Thus the singlet order of pyruvate hydrate created at low field is observed when the spectrum is acquired at high field. Note that the signal from the pyruvate hydrate formed at high field in Figure 5(c) is weaker than that observed in Figure 5(b). This may be due to the longer delay between dissolution and acquisition when the sample was shaken in the mu-metal chamber.

CONCLUSIONS

We have shown here that singlet order in hyperpolarized [1,2-$^{13}C_2$]pyruvate was longer lived than the longitudinal magnetization at low field, both in whole human blood *in vitro* and in a mouse *in vivo*. However, the benefit of creating singlet order in [1,2-$^{13}C_2$]pyruvate is limited by the relatively long T_1 for both carbons at high field, which in blood was between 1.5 and 2 times longer than T_S at low field. Furthermore, we have shown previously that, while the T_S for [1,2-$^{13}C_2$]pyruvate in D_2O buffer was approximately twice T_1^{LF} of the same molecule (13), it was not significantly longer than the T_1^{LF} of [1-^{13}C]pyruvate. To summarize: (i) the spin order of [1,2-$^{13}C_2$]pyruvate can be preserved effectively in blood at low field by using a long-lived singlet state; (ii) the long lifetime cannot, however, provide additional information on the metabolic conversion of pyruvate to lactate, since the singlet state is not preserved in the conversion of pyruvate to lactate. The advantage of generating the singlet state will only be realized for those doubly labeled molecules that possess lifetimes T_S that significantly exceed T_1 of the singly labeled isotopologues at both low *and* high magnetic fields.

Acknowledgements

The work was supported by a Cancer Research UK Programme grant (C197/A3514) and by a Translational Research Program Award from The Leukemia and Lymphoma Society to K. M. B. The authors I. M.-R. and E. M. S. acknowledge the European Union Seventh Framework Programme (FP7/2007-2013) for support under the Marie Curie Initial Training Network *METAFLUX* (project number 264780). T. B. R was in receipt of Intra-European Marie Curie and long-term EMBO fellowships. We are grateful to Professor R. Farndale and N. Pugh for experimental assistance. We are also grateful to Professor J. Metcalfe for helpful discussions.

REFERENCES

1. Vander Heiden MG, Cantley LC, Thompson CB. Understanding the Warburg effect: the metabolic requirements of cell proliferation. Science 2009; 324(5930): 1029–1033.
2. Brindle KM, Bohndiek SE, Gallagher FA, Kettunen MI. Tumor imaging using hyperpolarized ^{13}C magnetic resonance. Magn. Reson. Med. 2011; 66: 505–519.
3. Brindle K. New approaches for imaging tumour responses to treatment. Nat Rev Cancer 2008; 8(2): 94–107.
4. Day SE, Kettunen MI, Cherukuri MK, Mitchell JB, Lizak MJ, Morris HD, Matsumoto S, Koretsky AP, Brindle KM. Detecting response of rat C6 glioma tumors to radiotherapy using hyperpolarized [1-^{13}C]pyruvate and ^{13}C magnetic resonance spectroscopic imaging. Magn. Reson. Med. 2011; 65: 557–563.
5. Day SE, Kettunen MI, Gallagher FA, Hu D-E, Lerche M, Wolber J, Golman K, Ardenkjaer-Larsen JH, Brindle KM. Detecting tumor response to treatment using hyperpolarized ^{13}C magnetic resonance imaging and spectroscopy. Nat. Med. 2007; 13: 1382–1387.
6. Gallagher FA, Kettunen MI, Hu D-E, Jensen PR, in 't Zandt R, Karlsson M, Gisselsson A, Nelson SK, Witney TH, Bohndiek SE, Hansson G, Peitersen T, Lerche MH, Brindle KM. Production of hyperpolarized [1,4-$^{13}C_2$]malate from [1,4-$^{13}C_2$]fumarate is a marker of cell necrosis and treatment response in tumors. Proc. Natl Acad. Sci. USA 2009; 106: 19,801–19,806.
7. Kurhanewicz J, Vigneron DB, Brindle K, Chekmenev EY, Comment A, Cunningham CH, DeBerardinis RJ, Green GG, Leach MO, Rajan SS, Rizi RR, Ross BD, Warren WS, Malloy CR. Analysis of cancer metabolism by imaging hyperpolarized nuclei: prospects for translation to clinical research. Neoplasia 2011; 13: 81–97.
8. Witney TH, Kettunen MI, Day SE, Hu D-E, Neves AA, Gallagher FA, Fulton SM, Brindle KM. A comparison between radiolabeled fluorodeoxyglucose uptake and hyperpolarized ^{13}C-labeled pyruvate utilization as methods for detecting tumor response to treatment. Neoplasia 2009; 11: 574–582.
9. Witney TH, Kettunen MI, Hu D-E, Gallagher FA, Bohndiek SE, Napolitano R, Brindle KM. Detecting treatment response in a model

of human breast adenocarcinoma using hyperpolarised [1-^{13}C]pyruvate and [1,4-$^{13}C_2$]fumarate. Br. J. Cancer 2010; 103: 1400–1406.
10. Ardenkjaer-Larsen JH, Fridlund B, Gram A, Hansson G, Hansson L, Lerche MH, Servin R, Thaning M, Golman K. Increase in signal-to-noise ratio of >10,000 times in liquid-state NMR. Proc. Natl Acad. Sci. USA 2003; 100: 10,158–10,163.
11. Albers MJ, Bok R, Chen AP, Cunningham CH, Zierhut ML, Zhang VY, Kohler SJ, Tropp J, Hurd RE, Yen YF, Nelson SJ, Vigneron DB, Kurhanewicz J. Hyperpolarized ^{13}C lactate, pyruvate, and alanine: noninvasive biomarkers for prostate cancer detection and grading. Cancer Res. 2008; 68: 8607–8615.
12. Nelson SJ, Kurhanewicz J, Vigneron DB, Larson P, Harzstarck A, Ferrone M, van Criekinge M, Chang J, Bok R, Park I, Reed G, Carvajal L, Crane J, Ardenkjaer-Larsen JH, Chen A, Hurd R, Odegardstuen L-I, Tropp J. Proof of concept clinical trial of hyperpolarized C-13 pyruvate in patients with prostate cancer. Proc. Intl Soc. Mag. Reson. Med. 2012; 2: 274.
13. Tayler MCD, Marco-Rius I, Kettunen MI, Brindle KM, Levitt MH, Pileio G. Direct enhancement of nuclear singlet order by dynamic nuclear polarization. J. Am. Chem. Soc. 2012; 134: 7668–7671.
14. Ghosh RK, Kadlecek SJ, Ardenkjaer-Larsen JH, Pullinger BM, Pileio G, Levitt MH, Kuzma NN, Rizi RR. Measurements of the persistent singlet state of N_2O in blood and other solvents-potential as a magnetic tracer. Magn. Reson. Med. 2011; 66: 1177–1180.
15. Bornet A, Jannin S, Bodenhausen G. Three-field NMR to preserve hyperpolarized proton magnetization as long-lived states in moderate magnetic fields. Chem. Phys. Lett. 2011; 512: 151–154.
16. Pileio G, Carravetta M, Levitt MH. Storage of nuclear magnetization as long-lived singlet order in low magnetic field. Proc. Natl Acad. Sci. USA 2010; 107: 17,135–17,139.
17. Sarkar R, Vasos PR, Bodenhausen G. Singlet-state exchange NMR spectroscopy for the study of very slow dynamic processes. J. Am. Chem. Soc. 2007; 129: 328–334.
18. Tayler MCD, Levitt MH. Singlet nuclear magnetic resonance of nearly-equivalent spins. Phys. Chem. Chem. Phys. 2011; 13: 5556–5560.
19. Levitt MH. Singlet nuclear magnetic resonance. Annu. Rev. Phys. Chem. 2012; 63: 89–105.
20. Hurd RE, Chen A, Cunningham CH, Tropp J. Scalar coupling patterns in hyperpolarized spin systems: J_{CC} spectral pattern in hyperpolarized 1,2-[^{13}C]-pyruvate. A potential indirect measure of polarization. In: *Experimental Nuclear Magnetic Resonance Conference*, Pacific Grove, CA. 2009.
21. Lau JY, Chen AP, Gu YP, Cunningham CH. A calibration-based approach to real-time in vivo monitoring of pyruvate C1 and C2 polarization using the JCC spectral asymmetry. NMR Biomed. 2013. DOI: 10.1002/nbm.2942.
22. Tropp J Multiplet asymmetry and multi-spin order in liquid-state NMR spectra of hyperpolarized compounds. Proc. Intl Soc. Magn. Reson. Med. 2010; 18: 1026.
23. Janick PA, Hackney DB, Grossman RI, Asakura T. MR imaging of various oxidation states of intracellular and extracellular hemoglobin. Am. J. Neuroradiol. 1991; 12: 891–897.
24. Endre ZH, Kuchel PW. Viscosity of concentrated solutions and of human erythrocyte cytoplasm determined from NMR measurement of molecular correlation times. The dependence of viscosity on cell volume. Biophys. Chem. 1986; 24: 337–355.
25. Pullinger BM, Kadlecek SJ, Kuzma NN, Rizi RR. The influence of bovine serum albumin on the T_1 relaxation of [1-^{13}C]pyruvate – a study at low fields. Proc. Intl Soc. Magn. Reson. Med. 2011; 1514.
26. Moreno KX, Sabelhaus SM, Merritt ME, Sherry AD, Malloy CR. Competition of pyruvate with physiological substrates for oxidation by the heart: implications for studies with hyperpolarized [1-^{13}C]pyruvate. Am. J. Physiol. Heart Circ. Physiol. 2010; 298: H1556–1564.
27. Miéville P, Jannin S, Bodenhausen G. Relaxometry of insensitive nuclei: optimizing dissolution dynamic nuclear polarization. J. Magn. Reson. 2011; 210: 137–140.
28. Silvennoinen MJ, Kettunen MI, Kauppinen RA. Effects of hematocrit and oxygen saturation level on blood spin–lattice relaxation. Magn. Reson. Med. 2003; 49: 568–571.
29. Lin AL, Qin Q, Zhao X, Duong TQ. Blood longitudinal (T_1) and transverse (T_2) relaxation time constants at 11.7 Tesla. Magn. Reson. Mater Phys. 2012; 25: 245–249.
30. Tayler MCD, Levitt MH. Paramagnetic relaxation of nuclear singlet states. Phys. Chem. Chem. Phys. 2011; 13: 9128–9130.